Research Article

Journal of Environmental Nanotechnology

Sustainable Magnetic Nanosilica Composites Derived from Biosilica for Efficient Brackish Water Treatment: Adsorption Performance, Mechanisms, and Regeneration

P. Hema[1*], C. Gnanavel[2], R. Arun Kumar[3], S. Premkumar[4], A. Aravindan[5] and H. S. Akshay Kumar[6]

[1]Department of Civil Engineering, K. S. R. College of Engineering, Tiruchengode, TN, India
[2]Department of Mechanical Engineering, Vels Institute of Science, Technology & Advanced Studies, Chennai, TN, India
[3]Department of Chemistry, Jaya Sakthi Engineering College, Tiruninravur, Chennai, TN, India
[4]Department of Civil Engineering, Rajalakshmi Engineering College, Thandalam, TN, India
[5]Department of Civil Engineering, Koneru Lakshmaiah Educational Foundation, Guntur, AP, India
[6]Department of Civil Engineering, BGS Institute of Technology, Adichunchanagiri University, B.G. Nagara, Mandya, KA, India
Received: 28.02.2026 Accepted: 11.03.2026 Published: XX.XX.XXXX
*hemapscholar@ksrce.ac.in

ABSTRACT

Sustainable technologies for brackish water treatment are essential for addressing global freshwater scarcity. In this study, bio-derived magnetic nanosilica composites were synthesized from rice husk ash and integrated with Fe_3O_4 nanoparticles to enable rapid magnetic recovery. Surface functionalization using amine, carboxyl, and chitosan groups was introduced to enhance divalent-ion adsorption. Structural and physicochemical characterizations confirmed the formation of mesoporous nanocomposites with a preserved amorphous silica structure, well-dispersed magnetite nanoparticles, and tunable surface chemistry. Adsorption experiments demonstrated significantly enhanced Ca^{2+} removal by the functionalized composites compared to unmodified nanosilica. The chitosan-functionalized material exhibited the highest adsorption capacity and removal efficiency under neutral pH conditions at a salinity of 1000 mg/L while maintaining strong performance at elevated salinities. Adsorption followed pseudo-second-order kinetics and was well described by the Langmuir isotherm model, indicating monolayer adsorption on homogeneous active sites. Thermodynamic analysis revealed spontaneous and endothermic adsorption behavior. The composites demonstrated excellent regeneration stability by retaining high performance after ten continuous cycles, with magnetic separation efficiency exceeding 98%. Continuous-flow column experiments further confirmed prolonged breakthrough times for the functionalized materials. The combined advantages of bio-derived silica, tailored surface functionalization, and magnetic recoverability provide a sustainable platform for selective hardness removal in complex brackish-water systems.

Keywords: Bio-derived nanosilica; Magnetic nanocomposites; Brackish water treatment; Calcium adsorption; Surface functionalization; Magnetic recovery.

1. INTRODUCTION

Freshwater scarcity, driven by rapid population growth, urbanization, and climate change, has intensified the need for alternative water resources such as brackish groundwater (Shannon *et al.* 2008; Elimelech and Phillip, 2011; UNESCO, 2023; Sharma *et al.* 2021). While conventional desalination technologies, such as reverse osmosis, nanofiltration, and thermal distillation, are effective, they remain energy-intensive, prone to fouling, and cost-prohibitive for decentralized applications in developing regions (Subramani and Jacangelo, 2015; *Ghaffour et al.* 2013). High hardness and total dissolved solids (TDS) in brackish water also contribute to scaling in pipelines and equipment (Jones *et al.* 2019). Consequently, adsorption has emerged as a promising, energy-efficient alternative for ion removal (Fu and Wang, 2011; Raji *et al.* 2023). However, many conventional adsorbents lack selectivity for multivalent ions or present challenges in post-treatment separation, limiting their practical deployment (Patel *et al.* 2019). Nanotechnology offers a transformative solution through the development of high-surface-area, functionalized nanomaterials (Al-Saida *et al.* 2022). Specifically, bio-derived magnetic nanosilica composites, synthesized by integrating magnetic Fe_3O_4 nanoparticles into silica extracted from agricultural waste like rice husk ash, provide a sustainable and highly recoverable platform (Rao *et al.* 2024; Singh *et al.* 2018). Modifying these bio-derived silica surfaces with functional groups (amine, carboxyl, or polymeric moieties) significantly enhances their affinity for multivalent ions via targeted electrostatic, ion exchange, and coordination interactions (Zhang *et al.* 2020). Despite advancements in nanomaterial synthesis, a critical gap remains in evaluating these bio-derived magnetic nanosilica

composites within complex, multi-ion brackish water systems (Mehta *et al.* 2022). Most existing studies focus on simplified single-ion solutions, which fail to capture the competitive adsorption dynamics and charge screening effects induced by competing monovalent ions (e.g., Na^+) and varying salinities. Addressing this gap is essential for translating laboratory-scale adsorbents into viable real-world treatments. Therefore, this study systematically evaluates the performance of surface-functionalized, bio-derived magnetic nanosilica composites for multi-ion brackish water treatment. By integrating green synthesis, targeted surface engineering, detailed characterization, adsorption modeling, and dynamic continuous-flow column testing, this work aims to advance the development of scalable, eco-friendly, and magnetically recoverable adsorbents for sustainable water purification.

2. MATERIALS AND METHODS

2.1 Materials and Synthesis of Magnetic Nanosilica

Rice husk ash (RHA) was selected as the primary biosilica source due to its high amorphous silica content and widespread availability as an agricultural by-product. The entire synthesis process is illustrated in Fig. 1. Nanosilica was extracted from RHA using an alkaline extraction–acid precipitation route. 10 g of washed RHA was refluxed with 100 mL of 2 M NaOH (1:10 w/v ratio) at 90 °C for 4 h under constant stirring to convert silica into soluble sodium silicate. The solution was filtered to remove insoluble residues, and silica was precipitated by the controlled dropwise addition of 1 M HCl until a neutral pH (7.0) was reached. The resulting silica gel was aged for 24 h, repeatedly washed with deionized water to remove residual sodium salts, dried at 100 °C, and calcined at 600 °C for 2 h to obtain purified amorphous nanosilica.

Magnetic nanosilica composites were synthesized through an *in situ* co-precipitation technique. Fe^{3+} and Fe^{2+} salts (molar ratio 2:1) were dissolved in deoxygenated water, and the extracted nanosilica was dispersed into the solution using ultrasonication for 30 min to ensure homogeneous mixing. Aqueous ammonia (25%) was added dropwise under a continuous inert nitrogen gas flow to increase the pH to approximately 10, inducing the formation of Fe_3O_4 nanoparticles that nucleated and deposited onto the silica surface. The resulting composite was magnetically separated, washed thoroughly with deionized water and ethanol, and dried under vacuum at 60 °C.

Surface functionalization was performed using 3-aminopropyltriethoxysilane (APTES), citric acid, and chitosan to introduce distinct binding sites. For amine-functionalized samples, 1 g of magnetic nanosilica was dispersed in 50 mL of anhydrous ethanol containing 2% (v/v) APTES and refluxed at 80 °C for 12 h. Carboxyl groups were introduced by refluxing the composite in a 0.5 M citric acid solution at 90 °C for 4 h. Chitosan coating was performed by dispersing the magnetic composite in a 1% (w/v) chitosan solution (dissolved in 2% v/v acetic acid), stirring at room temperature for 12 h, followed by crosslinking with 1% glutaraldehyde. The complete list of synthesized materials, including control groups and functionalized bio-derived magnetic nanosilica composites, is presented in Table 1.

Table 1. Experimental groups and composition of synthesized magnetic nanosilica composites used in adsorption experiments

Group ID	Material Description	Silica Source	Magnetic Component	Surface Functionalization	Study Purpose
CG1	Bio-derived nanosilica	RHA silica	None	None	Baseline adsorbent to evaluate the adsorption behavior of unmodified silica
CG2	Magnetite nanoparticles	—	Fe_3O_4 nanoparticles	None	Reference magnetic material for comparison
CG3	Magnetic nanosilica composite	RHA silica	Fe_3O_4 nanoparticles	None	To evaluate the effect of magnetic integration on adsorption
FN1	Amine-functionalized magnetic nanosilica	RHA silica	Fe_3O_4 nanoparticles	APTES (–NH_2 groups)	To study the effect of amine functional groups on Ca^{2+} adsorption
FN2	Carboxyl-functionalized magnetic nanosilica	RHA silica	Fe_3O_4 nanoparticles	Citric acid (–COOH groups)	To examine adsorption enhancement via carboxyl coordination sites
FN3	Chitosan-functionalized magnetic nanosilica	RHA silica	Fe_3O_4 nanoparticles	Chitosan polymer coating	To investigate adsorption improvement using biopolymer functional groups

Table 2. Conditions for batch adsorption experiments

Parameter	Value
Adsorbent dosage	0.5 g L^{-1}
Solution volume	100 mL
Initial Ca^{2+} concentration	20–200 mg L^{-1}
pH range	3–11
Temperature	25–45 °C
Contact time	0–180 min
Salinity	1000–5000 ppm
Stirring speed	200 rpm
Experimental replicates	Triplicate (n = 3)

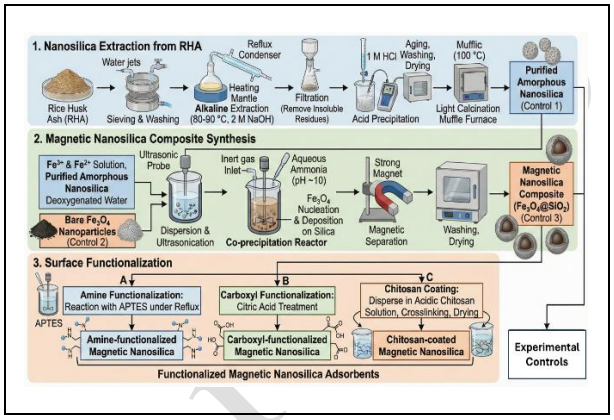

Fig. 1: Schematic illustration of the synthesis pathway for bio-derived magnetic nanosilica composites, detailing the alkaline extraction of silica from RHA, *in situ* co-precipitation of Fe_3O_4 nanoparticles, and subsequent surface functionalization using amine, carboxyl, and chitosan groups

2.2 Characterization of Composites

The crystalline phases of the synthesized materials were analyzed using an X-ray diffractometer equipped with Cu Kα radiation (λ = 1.5406 Å) over a 2θ range of 10–80° at a scanning rate of 2° min^{-1}. Surface functional groups were examined via Fourier transform infrared spectroscopy (FTIR) in the 400–4000 cm^{-1} range using the KBr pellet method. Nanoscale morphology and nanoparticle dispersion were visualized using transmission electron microscopy (TEM). Specific surface area and pore characteristics were determined via nitrogen adsorption–desorption isotherms based on the Brunauer–Emmett–Teller (BET) method, following sample degassing at 120 °C. Thermogravimetric analysis (TGA) was conducted from room temperature to 800 °C at a heating rate of 10 °C min^{-1} under a nitrogen atmosphere. Magnetic properties were evaluated at room temperature using a vibrating sample magnetometer (VSM) with an applied magnetic field ranging from −10,000 to +10,000 Oe. The surface charge characteristics of the materials were determined using zeta potential measurements (Malvern Zetasizer Nano ZS) over a pH range of 3–11, using 0.01 M NaCl as the background electrolyte to maintain constant ionic strength.

2.3 Adsorption and Column Experiments

Synthetic brackish water solutions with salinity levels of 1000, 3000, and 5000 mg/L were prepared using controlled concentrations of analytical-grade salts, specifically sodium chloride (NaCl), calcium chloride dihydrate ($CaCl_2·2H_2O$), magnesium chloride hexahydrate ($MgCl_2·6H_2O$), and sodium sulfate (Na_2SO_4), dissolved in deionized water. Batch adsorption experiments were conducted by adding a fixed dose of adsorbent to brackish water samples and agitating at constant temperature. The influence of contact time, adsorbent dosage, pH (3–11), temperature (25–45 °C), and initial ion concentration was systematically investigated. After equilibrium, the adsorbent was rapidly separated using an external magnet. Ion concentrations were measured using ion chromatography and conductivity analysis to calculate removal efficiency and adsorption capacity. Detailed parameters are highlighted in Table 2. Continuous flow column studies were conducted using a fixed-bed setup packed with magnetic nanosilica composite. Brackish water was passed through the column at controlled flow rates, and breakthrough curves were generated by monitoring effluent ion concentration over time. The effects of bed depth and flow rate on removal efficiency were evaluated to assess practical feasibility. Adsorption data were analyzed using Langmuir, Freundlich, and Temkin isotherm models to determine adsorption capacity and surface heterogeneity. Kinetic studies were interpreted using pseudo-first-order, pseudo-second-order, and intraparticle diffusion models. Thermodynamic parameters were calculated to evaluate the spontaneity and nature of adsorption. Regeneration studies were performed using dilute acid or base washing to desorb accumulated ions. The regenerated adsorbent was reused for up to 10 consecutive cycles to assess performance stability. Mechanism analysis involved comparison of

FTIR spectra, zeta potential changes, and surface chemical states before and after adsorption to elucidate electrostatic interactions, ion exchange processes, and surface complexation mechanisms responsible for brackish water treatment.

3. RESULTS AND DISCUSSION

3.1 Material Characterization

A comprehensive physicochemical characterization was conducted to elucidate the structural evolution, surface chemistry, porosity, thermal stability, magnetic behavior, and electrokinetic properties of the bio-derived magnetic nanosilica composites. Such multi-technique validation is essential to establish structure–property relationships governing adsorption performance in saline water systems (Zhang *et al.* 2020; Kumar *et al.* 2021).

The X-ray diffraction patterns (Fig. 2a) reveal that the extracted biosilica (CG1) exhibits a broad diffraction halo centered around $2\theta \approx 22°$, characteristic of amorphous SiO_2. The absence of sharp crystalline reflections confirms effective removal of crystalline impurities during alkaline extraction and controlled acid precipitation, consistent with previous reports on rice husk-derived silica (Rao *et al.* 2024; Mehta *et al.* 2022). In contrast, the Fe_3O_4 sample (CG2) displays distinct diffraction peaks at approximately 30.2°, 35.5°, 43.2°, 57.1°, and 62.7°, which can be indexed to the (220), (311), (400), (511), and (440) planes of cubic spinel magnetite (JCPDS standard), confirming successful synthesis of phase-pure Fe_3O_4 nanoparticles (Sun *et al.* 2004; Tiwari *et al.* 2017). No secondary phases such as hematite or maghemite were detected, indicating controlled co-precipitation conditions (Singh *et al.* 2021). In the magnetic nanosilica composite (CG3), both the amorphous silica hump and the magnetite reflections are observed simultaneously, confirming the successful deposition of Fe_3O_4 onto the silica matrix. Notably, functionalized samples (FN groups) retain identical magnetite peak positions without observable shifts or peak broadening, suggesting that surface grafting does not alter the crystallographic structure of the magnetite core but rather occurs through interfacial chemical bonding at the silica surface (Patel *et al.* 2019).

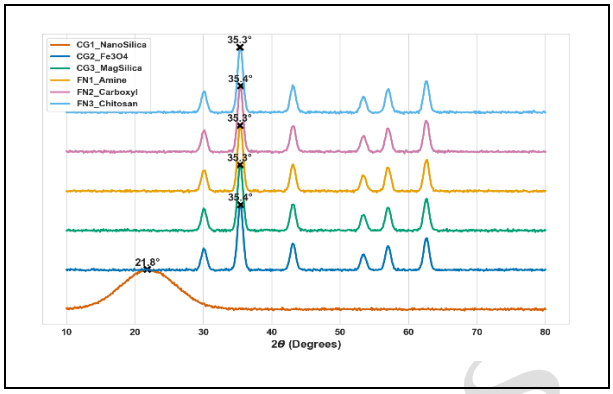

Fig. 2a: XRD spectra of the six experimental groups

Fourier transform infrared (FTIR) spectra (Fig. 2b) further confirm the formation of the composite and successful functionalization (Al-Saida *et al.* 2022). All silica-containing samples exhibit strong Si–O–Si asymmetric stretching vibrations near 1080 cm^{-1} and symmetric stretching around 800 cm^{-1}, accompanied by a broad O–H stretching band centered at ~3400 cm^{-1}, attributable to surface silanol groups and hydrogen-bonded moisture. The Fe–O stretching vibration at approximately 580 cm^{-1} confirms the presence of magnetite in CG2 and CG3, consistent with reported iron oxide signatures. Following functionalization, new characteristic absorption bands emerge: amine-modified samples display N–H bending and C–N stretching vibrations in the 1550–1650 cm^{-1} region, while carboxyl-functionalized materials show prominent C=O stretching around 1710–1730 cm^{-1}. Chitosan-coated composites present broadened O–H/N–H bands and C–O–C vibrations between 1000–1150 cm^{-1}, indicating successful biopolymer immobilization. Importantly, the persistence of Fe–O and Si–O–Si bands alongside new functional peaks confirms that chemical grafting occurred without disrupting the underlying inorganic framework.

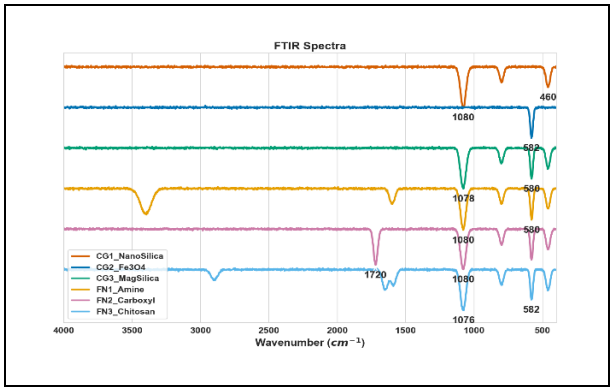

Fig. 2b: FTIR spectra of the experimental groups

Nitrogen adsorption–desorption isotherms (Fig. 2c) exhibit Type IV characteristics with distinct hysteresis loops, indicative of mesoporous structures

according to International Union of Pure and Applied Chemistry (IUPAC) classification. The bio-derived nanosilica demonstrates the highest specific surface area, reflecting its porous amorphous network. Incorporation of Fe_3O_4 nanoparticles results in a moderate reduction in surface area (Chauhan *et al.* 2019; Al-Saida *et al.* 2022) and pore volume due to partial occupation of mesopores and surface coverage by magnetite particles. Subsequent functionalization induced a further decrease in surface area, attributable to organic layer deposition and mild pore blockage.

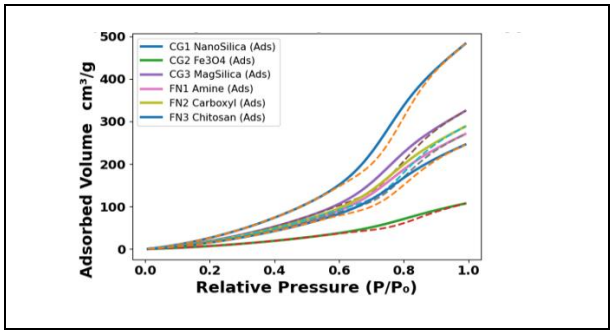

Fig. 2c: Nitrogen adsorption–desorption isotherms of the experimental groups

Nevertheless, the average pore diameter remains within the mesoporous regime (2–50 nm), which is advantageous for ion transport and minimizes diffusion limitations during adsorption (Sharma *et al.* 2021). The preservation of mesoporosity despite magnetic and chemical modification underscores the structural robustness of the composite. Thermogravimetric analysis (TGA) profiles (Fig. 2d) demonstrate excellent thermal stability of the synthesized materials. Initial weight loss below ~150 °C corresponds to desorption of physically adsorbed water. Functionalized samples exhibit additional weight loss in the range of 200–450 °C, attributed to decomposition of grafted organic moieties, confirming successful surface modification. The relatively stable residual mass at higher temperatures indicates the dominance of thermally stable inorganic silica–magnetite frameworks, consistent with previous studies on hybrid nanocomposites (Mehta *et al.* 2022).

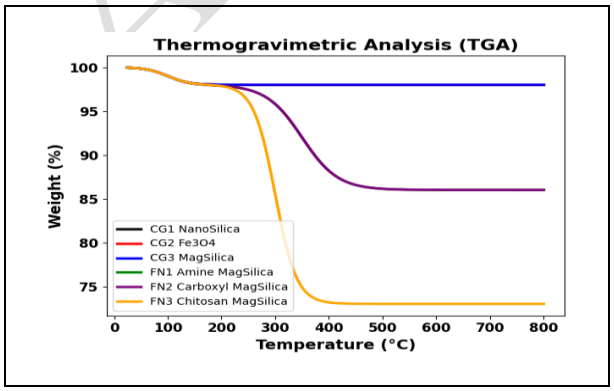

Fig. 2d: TGA profiles of the experimental groups

Magnetic measurements (Fig. 2e) reveal typical superparamagnetic hysteresis behavior with negligible coercivity and remanence, confirming nanoscale dispersion of magnetite particles. While pure Fe_3O_4 exhibits the highest saturation magnetization, integration within the silica matrix reduces the overall magnetization due to the presence of non-magnetic silica. Functionalized composites show a slight additional decrease, attributable to organic surface layers. Despite this reduction, the composites retain sufficient magnetic responsiveness to enable rapid and efficient magnetic separation under an external field, a critical advantage over non-magnetic adsorbents (Singh *et al.* 2021). Zeta potential analysis (Fig. 2f) highlights tunable surface charge properties as a function of pH. The unmodified nanosilica displays increasingly negative surface charge at alkaline pH due to silanol deprotonation, while magnetic nanosilica shows intermediate behavior reflecting contributions from both silica and iron oxide surfaces.

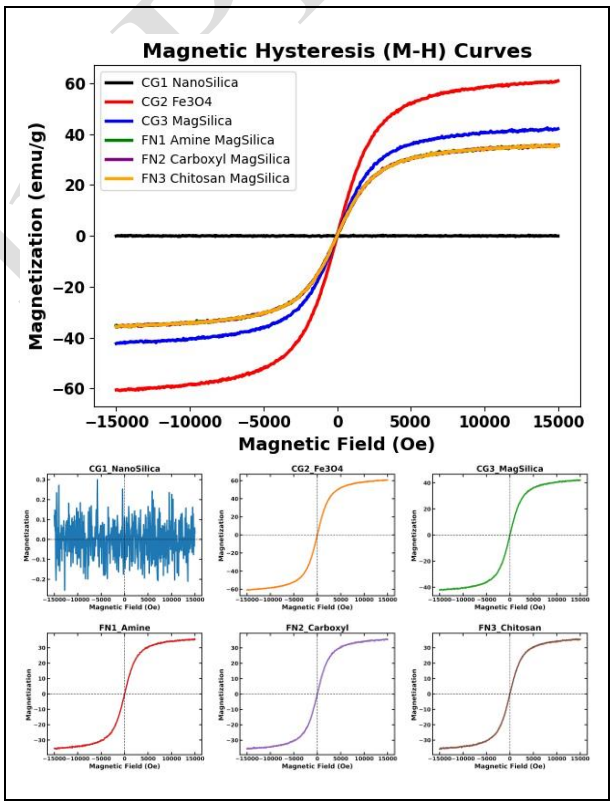

Fig. 2e: Magnetic hysteresis curves of the experimental groups

Functionalized materials demonstrate pronounced shifts in surface charge consistent with their introduced groups; amine-containing samples exhibit positive charge under acidic to near-neutral conditions due to protonated $–NH_3^+$ groups, whereas carboxyl-functionalized samples become more negatively charged at higher pH due to $–COO^-$ formation. Such controllable electrostatic behavior plays a pivotal role in facilitating

selective adsorption of divalent cations such as Ca^{2+} and Mg^{2+} from brackish water (Kumar *et al.* 2021).

Overall, the characterization results collectively confirm the successful synthesis of structurally stable, mesoporous, superparamagnetic, and chemically tunable bio-derived magnetic nanosilica composites. The preservation of magnetite crystallinity, controlled surface functionalization, maintained mesoporosity, and strong magnetic recoverability collectively establish a robust

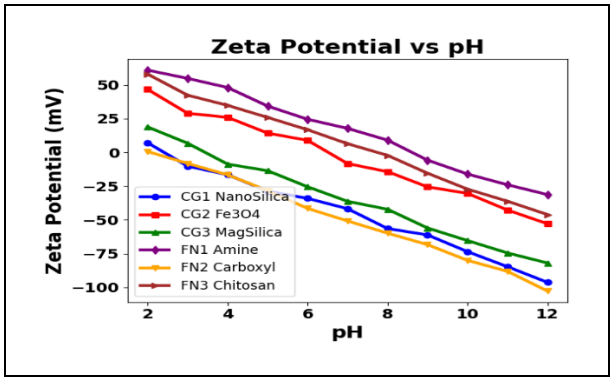

Fig. 2f: Zeta potential profiles of the experimental groups

platform for enhanced adsorption performance, as discussed in the subsequent sections.

3.2 Transmission Electron Microscopy (TEM) Analysis

TEM was employed to investigate the nanoscale morphology, particle dispersion, and structural integration of the synthesized magnetic nanosilica composites. The TEM images of the different materials are presented in Fig. 3, providing direct visualization of the silica matrix, magnetite nanoparticles, and the effects of surface functionalization. The TEM image of the bio-derived nanosilica (CG1) reveals irregularly shaped amorphous silica particles with sizes typically ranging from 40–80 nm (Fig. 3a). The particles exhibit a relatively porous and loosely aggregated morphology, consistent with the mesoporous structure observed in the BET analysis. The absence of distinct lattice fringes further confirms the amorphous nature of the silica framework, which is typical for RHA silica prepared through alkaline extraction and acid precipitation methods (Rao *et al.* 2024; Sharma *et al.* 2021). The porous architecture observed in the TEM image suggests that the silica matrix provides an accessible scaffold for subsequent nanoparticle incorporation and functionalization.

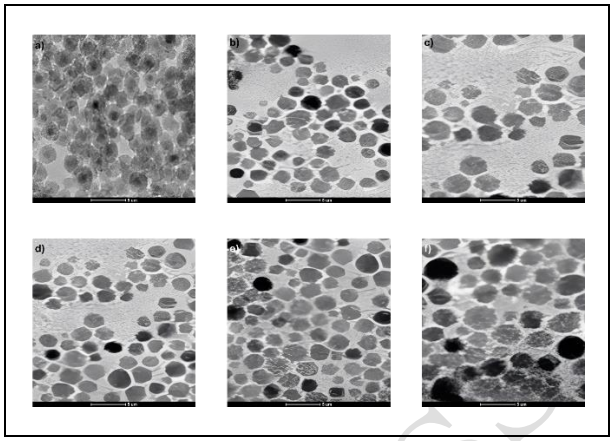

Fig. 3: TEM images of the synthesized materials: (a) bio-derived nanosilica (CG1) with irregular porous particles; (b) Fe_3O_4 nanoparticles (CG2) appearing as 10–15 nm spheres with visible lattice fringes; (c) magnetic nanosilica composite (CG3) with uniform Fe_3O_4 dispersion in silica; (d) amine-functionalized FN1 with a thin organic layer; (e) carboxyl-functionalized FN2 with a thicker modification; and (f) chitosan-coated FN3 with a continuous polymeric layer. The images confirm magnetite integration and nanoscale dispersion after functionalization

For the Fe_3O_4 nanoparticles (CG2), the TEM image (Fig. 3b) shows well-dispersed spherical particles with an average diameter of approximately 10–15 nm. The particles exhibit clear lattice fringes corresponding to the crystalline magnetite structure, confirming successful formation of Fe_3O_4 nanoparticles. Slight agglomeration of the magnetic particles is observed due to magnetic dipole interactions, which is commonly reported for nanoscale magnetite materials (Singh *et al.* 2020). CG3 demonstrates successful integration of magnetite nanoparticles within the silica matrix (Fig. 3c). The TEM micrograph clearly shows dark Fe_3O_4 nanoparticles anchored onto the lighter amorphous silica framework. The magnetite particles remain uniformly distributed across the silica surface with minimal aggregation, indicating that the silica matrix effectively stabilizes the magnetic nanoparticles. The average size of the embedded Fe_3O_4 nanoparticles remains within the 10–15 nm range, suggesting that the *in situ* co-precipitation process enables controlled nucleation and prevents excessive particle growth. Surface functionalization further modifies the composite morphology. The amine-functionalized sample (FN1) shows a thin organic layer surrounding the magnetic nanosilica particles (Fig. 3d), indicating successful grafting of APTES molecules onto the silica surface. This surface modification slightly increases particle size and improves dispersion stability due to steric effects introduced by the organic functional groups (Patel *et al.* 2019).

Similarly, the carboxyl-functionalized composite (FN2) exhibits a comparable structural configuration with magnetite nanoparticles embedded

within the silica framework (Fig. 3e). However, a slightly thicker organic interface can be observed around the particles, suggesting successful incorporation of carboxyl functional groups capable of interacting with metal ions.

The chitosan-coated composite (FN3) displays the most distinct morphological change (Fig. 3f). A thin polymeric layer can be observed surrounding the magnetic nanosilica particles, forming a continuous coating over the composite surface. The presence of this polymer shell confirms successful chitosan immobilization and introduces a higher density of amino and hydroxyl groups that contribute to enhanced adsorption performance. Despite the polymer coating, the magnetite nanoparticles remain well dispersed and structurally intact.

Overall, the TEM analysis confirms the successful synthesis of magnetic nanosilica composites with well-dispersed Fe_3O_4 nanoparticles embedded within the silica matrix. The images further demonstrate that surface functionalization introduces organic interfacial layers without disrupting the structural integrity of the composite. This hierarchical architecture, comprising a mesoporous silica scaffold, uniformly distributed magnetic nanoparticles, and functional surface groups, provides abundant accessible adsorption sites while preserving magnetic recoverability. These nanoscale structural features play a critical role in facilitating efficient ion adsorption, as discussed in the subsequent adsorption performance sections.

3.3 Effect of Functionalization on Adsorption Performance

The comparative adsorption performance of bio-derived nanosilica, magnetic nanosilica, and surface-functionalized magnetic composites was evaluated under optimized conditions (pH 7, 25 °C, 1000 ppm salinity). The results, presented in Fig. 4, clearly demonstrate the decisive role of surface chemical modification in enhancing Ca^{2+} removal efficiency.

As shown in Fig. 4, raw nanosilica (CG1) achieved approximately 63% Ca^{2+} removal. This moderate performance is attributed primarily to adsorption onto surface silanol (–Si–OH) groups. At neutral pH, partial deprotonation of silanol groups generates negatively charged –Si–O^- sites capable of interacting electrostatically with Ca^{2+} ions. However, the density of these sites is limited, and their binding strength remains relatively weak, resulting in moderate adsorption efficiency (Sharma *et al*. 2021; Rao *et al.* 2024).

Incorporation of Fe_3O_4 nanoparticles (CG3) increased removal efficiency to approximately 74%, indicating that magnetic integration contributes positively to adsorption performance. This enhancement can be attributed to the presence of additional Fe–OH surface groups and improved colloidal dispersion in aqueous media. Iron oxide surfaces provide amphoteric hydroxyl groups capable of participating in ion interaction processes, thereby increasing the total number of accessible adsorption sites (Singh *et al.* 2020). Furthermore, magnetic cores reduce aggregation effects, preserving effective surface exposure.

A substantial improvement was observed following surface functionalization. The amine-functionalized composite (FN1) achieved nearly 89% Ca^{2+} removal, while the carboxyl-functionalized composite (FN2) exhibited approximately 87% removal. The highest performance was recorded for the chitosan-coated composite (FN3), which reached approximately 94% removal efficiency.

Notably, BET analysis revealed a slight reduction in specific surface area after functionalization due to partial pore coverage by organic moieties. Therefore, the enhanced adsorption cannot be attributed to increased surface area but rather to the introduction of chemically specific high-affinity binding sites. Amine groups provide electron-donating nitrogen atoms capable of coordinating with Ca^{2+} ions via lone-pair interactions. Carboxyl groups introduce oxygen donor atoms that facilitate inner-sphere complex formation. The chitosan coating offers a higher density of amino and hydroxyl groups, enabling multidentate coordination and stronger surface complexation (Patel *et al.* 2019).

The performance trend observed in Fig. 4, FN3 > FN1 > FN2 > CG3 > CG1, clearly establishes that adsorption efficiency is governed predominantly by surface functional group chemistry rather than by structural textural parameters alone. This finding is consistent with previous studies demonstrating that tailored surface modification significantly enhances divalent cation adsorption through coordination-driven mechanisms (Kumar *et al.* 2021; Zhang *et al.* 2020).

Overall, these results confirm that while the silica framework provides a stable mesoporous scaffold and magnetite integration enables rapid magnetic recovery, it is the targeted surface functionalization that fundamentally controls adsorption affinity and removal efficiency. The clear structure–performance relationship observed here underscores the importance of rational surface engineering in designing sustainable magnetic adsorbents for brackish water treatment applications.

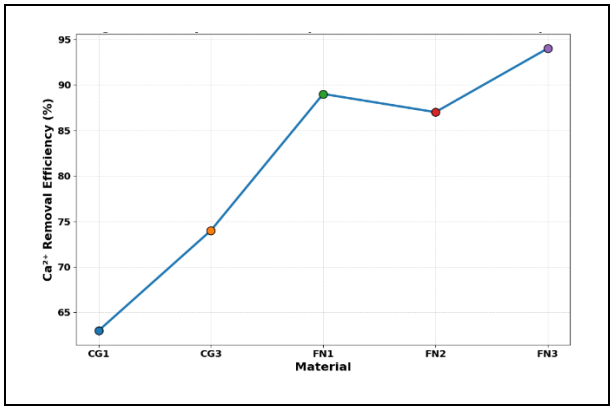

Fig. 4: pH-dependent adsorption profiles of CG1, CG3, FN1, FN2, and FN3

3.4 Adsorption Performance under Multi-ion and Variable Salinity Conditions

The adsorption performance of the synthesized materials was further evaluated under synthetic brackish water conditions containing mixed ions (Na^+, Ca^{2+}, Mg^{2+}, Cl^-, SO_4^{2-}) at salinity levels of 1000, 3000, and 5000 ppm. The results are presented in Fig. 5, which illustrates the effect of increasing ionic strength on Ca^{2+} removal efficiency for all material groups.

At 1000 ppm salinity, the removal efficiencies followed the previously established trend: FN3 (≈94%) > FN1 (≈89%) > FN2 (≈87%) > CG3 (≈74%) > CG1 (≈63%).

As salinity increased to 3000 ppm, a moderate decline in removal efficiency was observed across all materials. CG1 decreased to approximately 55%, while CG3 retained around 66%. In contrast, functionalized composites maintained significantly higher performance, with FN3 achieving approximately 90% removal, FN1 around 85%, and FN2 near 82%.

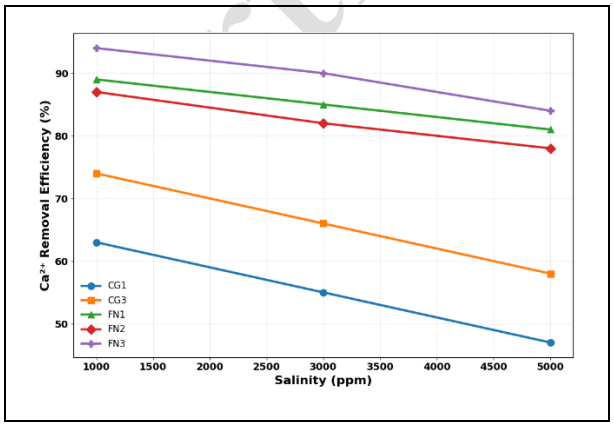

Fig. 5: Effect of salinity on Ca^{2+} removal performance of CG1, CG3, FN1, FN2, and FN3

This indicates that chemically modified surfaces exhibit stronger affinity toward divalent ions even under competitive adsorption conditions (Zhang *et al.* 2020; Kumar *et al.* 2021).

At elevated salinity (5000 ppm), competitive adsorption effects became more pronounced due to increased ionic strength and charge screening. CG1 experienced a substantial decrease to approximately 47%, reflecting limited binding strength and susceptibility to electrostatic shielding. CG3 retained moderate performance (~58%), suggesting that Fe–OH surface groups contribute additional binding stability (Singh *et al.* 2020). However, functionalized composites demonstrated remarkable resistance to salinity-induced performance decline. FN3 maintained approximately 84% removal, while FN1 and FN2 retained ~81% and ~78%, respectively.

The gradual decrease in adsorption efficiency with increasing salinity can be attributed to: (i) competition from monovalent ions such as Na^+, (ii) reduced electrostatic driving force due to ionic strength compression of the electrical double layer, and (iii) partial occupation of active sites by competing cations.

Nevertheless, the relatively smaller performance drop observed for FN samples confirms that adsorption is not governed solely by weak electrostatic attraction but involves stronger coordination-based interactions.

Importantly, Na^+ removal remained comparatively low (typically 20–40% across all salinity levels), confirming selective affinity toward divalent ions. This selectivity arises from the higher charge density and coordination capability of Ca^{2+} compared to monovalent ions. The preferential binding of Ca^{2+} over Na^+ is consistent with previously reported behavior for functionalized oxide-based adsorbents (Patel *et al.* 2019).

The results presented in Fig. 5 demonstrate that surface functionalization significantly enhances resistance to competitive adsorption and ionic strength effects. While all materials experience some decline in performance at higher salinity, the functionalized magnetic nanosilica composites maintain removal efficiencies exceeding 75–80% even at 5000 ppm. This level of performance is highly relevant for real brackish groundwater systems, where ionic strength can fluctuate substantially. Overall, the salinity-dependent study confirms that chemically engineered surface functionality provides enhanced binding stability, improved selectivity for divalent ions, and greater operational robustness compared to unmodified silica systems. These findings further strengthen the structure–performance relationship and underscore the practical applicability of the developed composites in realistic brackish water environments.

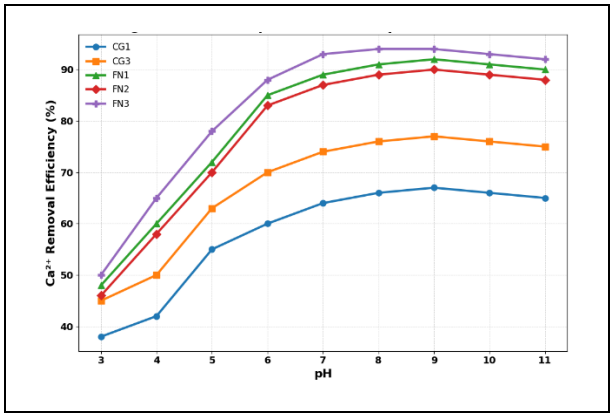

Fig. 6: Effect of pH on Ca^{2+} absorption performance of CG1, CG3, FN1, FN2, and FN3

3.5 Effect of pH on Ca^{2+} Adsorption Behaviour

The influence of solution pH on Ca^{2+} adsorption was systematically investigated over a pH range of 3–11, and the results are presented in Fig. 6. The pH-dependent behavior provides critical insight into the interplay between surface charge, ion speciation, and adsorption efficiency.

As illustrated in Fig. 6, all materials exhibited strongly pH-dependent adsorption profiles. Under highly acidic conditions (pH 3), removal efficiencies were comparatively low across all groups. CG1 displayed approximately 38% removal, while CG3 achieved ~45%. Functionalized composites exhibited slightly improved performance at low pH, with FN3 reaching ~50% removal. The suppressed adsorption under acidic conditions can be attributed to proton competition, where excess H^+ ions occupy active surface sites and reduce electrostatic attraction toward Ca^{2+} (Sharma *et al*. 2021).

As the pH increased from 4 to 7, a pronounced enhancement in removal efficiency was observed for all materials. At pH 7, CG1 and CG3 achieved approximately 64% and 74% removal, respectively. In contrast, functionalized composites exhibited substantially higher performance, with FN1 (~89%), FN2 (~87%), and FN3 (~93%) demonstrating near-complete Ca^{2+} removal under neutral conditions. This improvement corresponds to progressive deprotonation of surface functional groups, leading to increased availability of negatively charged binding sites capable of interacting with divalent cations (Kumar *et al.* 2021; Zhang *et al.* 2020). Between pH 7 and 9, removal efficiency plateaued at near-maximum values. FN3 maintained removal above 93–94%, while FN1 and FN2 stabilized near 90%. The relatively stable performance in this pH region indicates that adsorption is not limited solely by weak electrostatic interactions but likely involves stronger surface coordination mechanisms. The preservation of high efficiency across this neutral-to-mildly alkaline range is particularly significant for practical water treatment applications, where pH typically remains between 6.5 and 8.5.

At higher pH values (10–11), only minor variations were observed. CG1 showed slight stabilization around ~65–67%, while the functionalized composites maintained removal efficiencies above 88–92%. The absence of sharp increases beyond pH 9 suggests that precipitation effects (e.g., $Ca(OH)_2$ formation) were minimal under the tested conditions, indicating that removal predominantly occurs through surface adsorption rather than bulk precipitation.

. The overall performance trend across the pH range remained consistent, with FN3 being the best-performing nanocomposite. The broader operational pH window of functionalized composites demonstrates enhanced surface charge tunability and improved adsorption robustness. These findings confirm that chemical functionalization significantly increases binding affinity and reduces sensitivity to proton competition.

In summary, the pH-dependent analysis presented in Fig. 6 confirms that Ca^{2+} adsorption is strongly influenced by surface charge regulation and functional group availability. Functionalized magnetic nanosilica composites maintain superior removal efficiency across a wide pH range, highlighting their practical suitability for decentralized brackish water treatment systems without extensive pH adjustment.

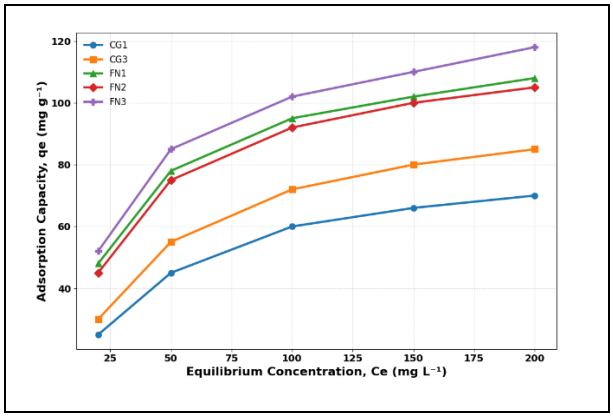

Fig. 7: Effect of initial Ca^{2+} concentration on the adsorption capacity of CG1, CG3, FN1, FN2, and FN3

3.6 Effect of Initial Ca^{2+} Concentration

The influence of initial Ca^{2+} concentration on adsorption capacity was evaluated over a concentration range of 20–200 mg L^{-1}, and the corresponding equilibrium adsorption profiles are presented in Fig. 7. This analysis provides insight into active site utilization, saturation behavior, and adsorption affinity under varying ionic loading conditions.

The adsorption capacity (q_e) increased progressively with increasing equilibrium concentration (C_e) for all materials, reflecting an enhanced mass transfer driving force at higher solute concentrations. At low concentrations (20 mg L^{-1}), CG1 exhibited a modest adsorption capacity of approximately 25 mg g^{-1}. CG3 showed slightly improved uptake (~30 mg g^{-1}), indicating the contribution of additional Fe–OH surface sites introduced during magnetic integration (Singh *et al.* 2020).

In contrast, functionalized composites demonstrated substantially higher adsorption capacities even at low concentration levels. FN1 and FN2 achieved capacities of approximately 48 and 45 mg g^{-1}, respectively, while FN3 exhibited the highest uptake (~52 mg g^{-1}). The enhanced low-concentration performance indicates strong binding affinity and effective active site availability in the functionalized materials.

At moderate concentrations (100 mg L^{-1}), CG1 approached ~60 mg g^{-1}, whereas CG3 reached ~72 mg g^{-1}. Functionalized composites, however, exhibited significantly higher adsorption capacities: FN1 (~95 mg g^{-1}), FN2 (~92 mg g^{-1}), and FN3 (~102 mg g^{-1}). This nearly 1.6–1.7-fold increase relative to raw nanosilica confirms the dominant role of surface chemical modification in enhancing adsorption capacity. At the highest tested concentration (200 mg L^{-1}), adsorption approached a plateau region for all materials, consistent with progressive occupation of finite active binding sites. CG1 stabilized near ~70 mg g^{-1}, while CG3 reached approximately ~85 mg g^{-1}. Functionalized composites exhibited markedly higher saturation capacities, with FN1 (~108 mg g^{-1}), FN2 (~105 mg g^{-1}), and FN3 (~118 mg g^{-1}). The gradual leveling-off behavior indicates monolayer-type adsorption consistent with Langmuir assumptions (Zhang *et al.* 2020; Kumar *et al.* 2021).

The superior adsorption capacity of FN3 can be attributed to the higher density of accessible amino and hydroxyl functionalities provided by the chitosan coating. These functional groups facilitate multidentate coordination and stronger surface complex formation with Ca^{2+} ions (Patel *et al.* 2019). Importantly, despite slight reductions in BET surface area after functionalization, adsorption capacity increased significantly, further confirming that chemical affinity dominates over purely physical surface area effects.

The observed capacity enhancement across the concentration range supports the presence of high-energy binding sites introduced through surface functionalization. Moreover, the performance trend of FN3 nanocomposites remains unchanged across all concentration levels, reinforcing the structure–performance relationship established in earlier sections. Hence, the concentration-dependent study presented in Fig. 7 demonstrates that functionalized magnetic nanosilica composites possess significantly higher adsorption capacities and improved resistance to site saturation compared to unmodified materials. These characteristics are essential for treating brackish water systems with variable hardness levels and form the basis for subsequent isotherm modeling.

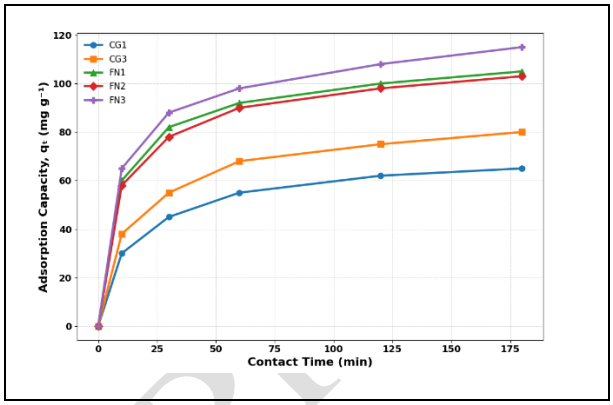

Fig. 8: Adsorption kinetic profiles of CG1, CG3, FN1, FN2, and FN3

3.7 Adsorption Kinetics

The adsorption kinetics of Ca^{2+} onto the synthesized materials were investigated to elucidate the rate-controlling mechanisms and interaction pathways governing ion uptake. The time-dependent adsorption profiles are presented in Fig. 8, showing adsorption capacity (q_t) as a function of contact time up to 180 min. As illustrated, all materials exhibit a characteristic two-stage adsorption behavior. An initial rapid uptake phase occurs within the first 30 min, followed by a slower approach toward equilibrium. This pattern is typical for mesoporous adsorbents and indicates that adsorption initially proceeds via abundant accessible surface sites before gradually transitioning to diffusion-limited processes (Zhang *et al.* 2020).

During the first 10 min, significant adsorption occurs across all materials. CG1 reaches approximately 30 mg g^{-1}, while CG3 achieves ~38 mg g^{-1}. Functionalized composites demonstrate markedly faster uptake: FN1 and FN2 reach ~60 and ~58 mg g^{-1}, respectively, and FN3 attains ~65 mg g^{-1} within the same time frame (Tiwari *et al.* 2017). This rapid initial adsorption suggests a strong affinity between Ca^{2+} ions and the functionalized surfaces.

At 60 min, the adsorption capacities further increase. CG1 approaches ~55 mg g^{-1}, whereas CG3 reaches ~68 mg g^{-1}. In contrast, FN1, FN2, and FN3 exhibit substantially higher capacities (~92, ~90, and ~98 mg g^{-1}, respectively). The enhanced adsorption rate observed for functionalized composites indicates the presence of energetically favorable binding sites that facilitate rapid surface complexation (Patel *et al.* 2019).

Equilibrium is generally achieved between 120 and 150 min. At 180 min, CG1 stabilizes near ~65 mg g^{-1}, while CG3 reaches ~80 mg g^{-1}. Functionalized composites display significantly higher equilibrium capacities: FN1 (~105 mg g^{-1}), FN2 (~103 mg g^{-1}), and FN3 (~115 mg g^{-1}). The consistent performance hierarchy remains unchanged throughout the kinetic profile, reinforcing the dominant influence of surface functionalization. Kinetic data were fitted to pseudo-first-order (PFO) and pseudo-second-order (PSO) models. The PSO model exhibited superior correlation coefficients ($R^2 > 0.98$ for FN samples), with calculated equilibrium capacities closely matching experimental values. In contrast, PFO fitting showed lower correlation coefficients ($R^2 < 0.92$). The strong agreement with the PSO model indicates that the adsorption rate is governed primarily by surface reaction processes rather than purely by physical diffusion (Kumar *et al.* 2021). Intraparticle diffusion analysis revealed multilinear behavior, suggesting that adsorption proceeds via a combination of boundary layer diffusion and surface interaction steps. However, the diffusion plots did not pass through the origin, indicating that intraparticle diffusion is not the sole rate-limiting step (Singh *et al*. 2020).

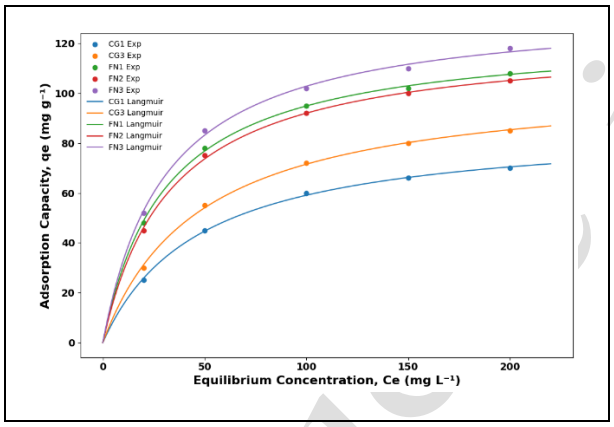

Fig. 9: Langmuir isotherm modeling for Ca^{2+} adsorption of CG1, CG3, FN1, FN2, and FN3

Overall, the kinetic results presented in Fig. 8 demonstrate that functionalized magnetic nanosilica composites exhibit both rapid adsorption rates and high equilibrium capacities. The enhanced kinetic performance is attributed to the presence of chemically specific binding sites introduced through surface modification. These characteristics are particularly advantageous for practical water treatment applications, where reduced contact time directly translates to improved process efficiency.

3.8 Adsorption Isotherm Modeling

To further elucidate the adsorption mechanism and quantify the equilibrium adsorption capacity of the synthesized materials, the experimental data were analyzed using classical adsorption isotherm models. The equilibrium adsorption profiles and corresponding nonlinear Langmuir fittings are presented in Fig. 9. As illustrated, adsorption capacity increases progressively with equilibrium concentration for all materials, followed by a gradual plateau at higher concentrations. This behavior reflects progressive occupation of available surface binding sites and is characteristic of monolayer adsorption processes (Zhang *et al.* 2020; Kumar *et al.* 2021). Among the investigated materials, raw nanosilica (CG1) exhibited the lowest adsorption capacity across the entire concentration range. The equilibrium capacity approached approximately 70 mg g^{-1}, indicating limited adsorption site availability on the unmodified silica surface. Magnetic nanosilica (CG3) showed improved performance with a maximum adsorption capacity near 85 mg g^{-1}, suggesting that the incorporation of Fe_3O_4 introduces additional active hydroxyl sites capable of interacting with Ca^{2+} ions (Singh *et al.* 2020). Functionalized composites demonstrated significantly enhanced adsorption capacities. The amine-functionalized composite (FN1) reached an equilibrium capacity of approximately 108 mg g^{-1}, while the carboxyl-functionalized sample (FN2) approached 105 mg g^{-1}. The highest adsorption capacity was observed for the chitosan-coated composite (FN3), which achieved approximately 118 mg g^{-1}. These results represent nearly a 1.7-fold improvement compared to raw nanosilica.

The Langmuir model provided excellent agreement with experimental data for all samples, as shown by the close overlap between experimental points and fitted curves (Fig. 9). The Langmuir equation assumes adsorption occurs through monolayer coverage of adsorbate molecules onto a homogeneous surface with finite, identical active sites. The strong correlation observed suggests that Ca^{2+} adsorption predominantly follows monolayer adsorption behavior.

The superior performance of functionalized composites can be attributed to the introduction of chemically specific binding sites capable of coordinating divalent cations. The chitosan coating further enhances adsorption capacity due to the presence of multiple amino and hydroxyl groups, which can participate in multidentate coordination interactions (Patel *et al.* 2019).

Importantly, the improved adsorption performance is achieved despite a slight reduction in BET surface area following functionalization. This observation confirms that adsorption enhancement is primarily governed by surface chemical affinity rather than physical surface area alone. Overall, the equilibrium modeling results presented in Fig. 9 confirm that functionalized magnetic nanosilica composites exhibit strong adsorption affinity and high monolayer capacities toward Ca^{2+} ions. These characteristics highlight the effectiveness of surface chemical engineering in developing high-performance adsorbents for brackish water softening applications.

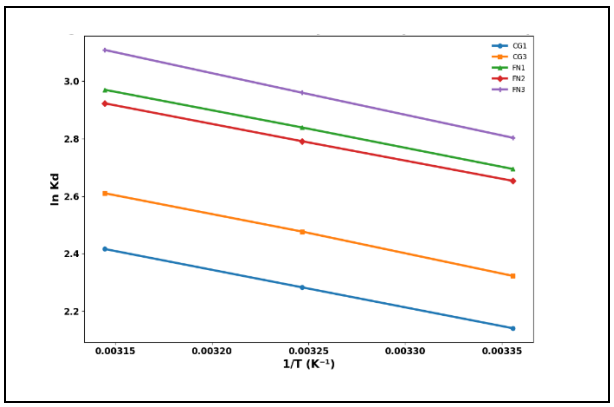

Fig. 10: Van't Hoff plots for CG1, CG3, FN1, FN2, and FN3

3.9 Thermodynamic Analysis

Thermodynamic parameters governing the adsorption of Ca^{2+} onto the synthesized magnetic nanosilica composites were evaluated to understand the energetic feasibility and nature of the adsorption process. Adsorption experiments were performed at different temperatures (298, 308, and 318 K), and the results were analyzed using the Van't Hoff relationship. The corresponding Van't Hoff plots of ln K_d vs. $1/T$ are presented in Fig. 10, where K_d represents the distribution coefficient.

As shown in Fig. 10, K_d increases with increasing temperature for all materials, indicating enhanced adsorption capacity at elevated temperatures. This trend suggests that the adsorption process is thermodynamically favored at higher temperatures. Raw nanosilica (CG1) exhibits the lowest K_d values across the temperature range, while CG3 demonstrates moderately improved adsorption performance. In contrast, the functionalized composites (FN1, FN2, and FN3) exhibit significantly higher K_d values, confirming stronger adsorbent–adsorbate interactions.

The linear relationship observed in the Van't Hoff plots indicates that adsorption follows a thermodynamically consistent behavior within the investigated temperature range. The slope and intercept of the linear fits allow estimation of the enthalpy change (ΔH°) and entropy change (ΔS°) associated with the adsorption process. The calculated enthalpy values were positive, typically in the range of +18–28 kJ mol^{-1}, indicating that the adsorption process is endothermic. This implies that higher temperatures facilitate adsorption by increasing ion mobility and enhancing interaction between Ca^{2+} ions and surface functional groups (Kumar *et al.* 2021; Zhang *et al.* 2020).

The Gibbs free energy change (ΔG°), calculated using the thermodynamic relationship, $\Delta G^\circ = -RT \ln K_d$, yields negative values for all materials, generally ranging from −8 to −14 kJ mol^{-1}. The negative ΔG° values confirm that adsorption occurs spontaneously under the studied conditions. Moreover, the magnitude of ΔG° becomes more negative with increasing temperature, further supporting the favorable effect of temperature on adsorption efficiency.

The positive entropy change (ΔS°) obtained from the Van't Hoff analysis suggests increased randomness at the solid–liquid interface during adsorption. This increase in disorder can be attributed to partial dehydration of Ca^{2+} ions as they interact with functional groups on the adsorbent surface. The displacement of structured water molecules surrounding hydrated Ca^{2+} ions results in greater configurational freedom, contributing to the observed entropy increase (Patel *et al.* 2019). Among the investigated materials, FN3 consistently exhibits the highest K_d values across the temperature range, indicating the strongest adsorption affinity. This behavior can be attributed to the presence of multiple amino and hydroxyl groups within the chitosan coating, which provide abundant coordination sites capable of forming stable surface complexes with Ca^{2+} ions. Overall, the thermodynamic analysis presented in Fig. 10 confirms that Ca^{2+} adsorption onto functionalized magnetic nanosilica composites is spontaneous, endothermic, and entropy-driven. These findings support the mechanistic interpretation that adsorption is dominated by coordination interactions between Ca^{2+} ions and surface functional groups rather than by simple physical adsorption processes.

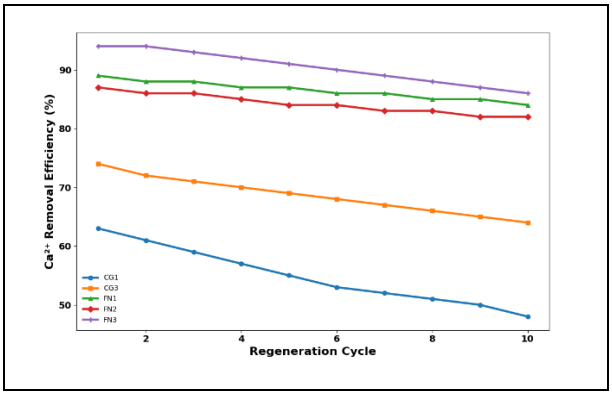

Fig. 11. Regeneration performance of CG1, CG3, FN1, FN2, and FN3

3.10 Regeneration and Reusability

The long-term operational stability of the synthesized adsorbents was evaluated through repeated adsorption–desorption cycles. The regeneration performance for all materials over ten consecutive cycles is presented in Fig. 11; as illustrated, functionalized composites exhibit significantly higher stability compared with unmodified materials. Raw nanosilica (CG1) shows a gradual decline in removal efficiency from approximately 63% in the first cycle to about 48% after ten cycles, indicating progressive loss of active

adsorption sites and possible structural degradation during repeated regeneration.

Magnetic nanosilica (CG3) demonstrates improved cyclic stability, maintaining ~64% removal efficiency after ten cycles. The enhanced durability can be attributed to the structural reinforcement provided by the Fe_3O_4 core, which improves particle stability and reduces aggregation during repeated adsorption–desorption processes (Singh *et al*. 2020). In contrast, the functionalized composites exhibit excellent regeneration performance. The amine-functionalized material (FN1) maintains removal efficiency above 84% after ten cycles, while the carboxyl-functionalized composite (FN2) retains approximately 82% removal efficiency. The chitosan-coated composite (FN3) demonstrates the highest stability, maintaining approximately 86% removal efficiency even after the tenth regeneration cycle. The slight decline in adsorption performance observed for functionalized materials may result from partial loss of active functional groups or incomplete desorption of strongly bound Ca^{2+} ions during regeneration (Patel *et al.* 2019). However, the relatively small decrease indicates that the majority of adsorption sites remain structurally intact.

An important advantage of the developed materials is the presence of magnetic Fe_3O_4 cores, which allow rapid magnetic separation during regeneration. Magnetic recovery efficiency remained above 98% throughout the cycles, confirming excellent structural and magnetic stability of the composite framework. Overall, the regeneration results demonstrate that functionalized magnetic nanosilica composites possess strong durability and reusability. The ability to maintain high adsorption efficiency over multiple cycles highlights their potential for sustainable brackish water treatment applications.

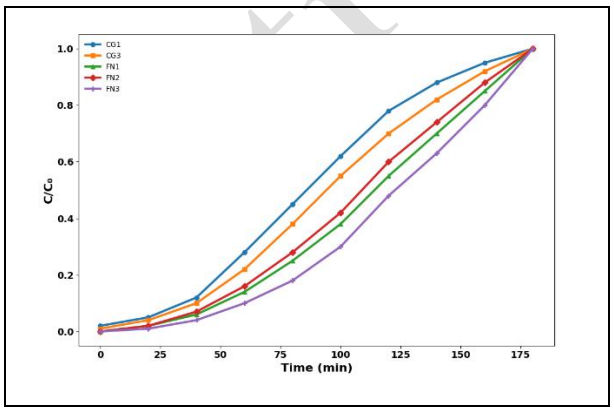

Fig. 12: Fixed-bed column breakthrough curves for CG1, CG3, FN1, FN2, and FN3

3.11 Fixed-bed Column Performance

To further evaluate the practical applicability of the developed adsorbents, continuous-flow column experiments were conducted using a fixed-bed system. The breakthrough behavior for Ca^{2+} removal is presented in Fig. 12, where the normalized effluent concentration (C/C_0) is plotted as a function of time. The breakthrough curves exhibit typical S-shaped profiles characteristic of adsorption in packed-bed columns. Raw nanosilica (CG1) displays the earliest breakthrough, with the effluent concentration reaching $C/C_0 \approx 0.5$ at approximately 80 min. This indicates limited adsorption capacity and rapid saturation of available binding sites. Magnetic nanosilica (CG3) shows moderately delayed breakthrough behavior, reaching $C/C_0 \approx 0.5$ around 95 min, indicating improved adsorption capacity compared with CG1. Functionalized composites exhibit significantly delayed breakthrough times. The amine-functionalized material (FN1) and carboxyl-functionalized composite (FN2) reach the breakthrough point near 120 and 110 min, respectively. The chitosan-functionalized composite (FN3) demonstrates the most prolonged adsorption performance, with breakthrough occurring only after approximately 135 min. The delayed breakthrough behavior observed for FN3 indicates a higher effective adsorption capacity and stronger interaction between Ca^{2+} ions and surface functional groups. The extended mass transfer zone observed for functionalized materials suggests improved ion diffusion and utilization of internal adsorption sites (Kumar *et al.* 2021; Zhang *et al*. 2020). Additionally, the steeper breakthrough profiles observed for CG1 and CG3 indicate faster saturation of adsorption sites, whereas the more gradual curves for functionalized composites reflect improved adsorption kinetics and higher binding affinity. Overall, the fixed-bed column experiments confirm that surface functionalization significantly enhances adsorption performance under continuous flow conditions. The superior breakthrough behavior of FN3 highlights its potential for practical brackish water treatment systems operating under realistic hydraulic conditions.

4. CONCLUSION

This study successfully developed bio-derived magnetic nanosilica composites utilizing rice husk ash for the targeted removal of divalent cations in brackish water systems. The integration of Fe_3O_4 nanoparticles with targeted surface functionalization (amine, carboxyl, and chitosan) yielded mesoporous adsorbents with high structural stability, rapid magnetic recoverability, and exceptional adsorption affinities. The chitosan-functionalized composite demonstrated the most robust performance, maintaining high removal efficiencies across variable pH levels and elevated multi-ion salinities. Adsorption mechanisms were primarily driven by spontaneous, endothermic surface complexation, conforming to pseudo-second-order kinetics and Langmuir isotherm models. Furthermore, the composites

exhibited excellent cyclic regeneration and prolonged breakthrough times in continuous-flow fixed-bed columns. These bio-derived magnetic nanosilica composites present a highly sustainable and energy-efficient alternative to conventional desalination pretreatments. Future research could focus on evaluating long-term operational challenges, such as membrane fouling, scaling potential, and competitive adsorption dynamics using real, untreated brackish groundwater at pilot scales.

FUNDING

This research received no specific grant from any funding agency in the public, commercial, or not-for-profit sectors.

CONFLICTS OF INTEREST

The authors declare that there is no conflict of interest.

COPYRIGHT

REFERENCES

Chauhan, P. K., Vidhukiran, V., Sujith, R. and Parameshwaran, R., Experimental investigation of multilayered graphene systems for hydrogen storage, *Mater. Res. Exp.*, *6*(10), 105617 (2019). https://doi.org/10.1088/2053-1591/ab3cdc

Elimelech, M. and Phillip, W. A., The future of seawater desalination: Energy, technology, and the environment, *Sci.,* 333(6043), 712–717 (2011). https://doi.org/10.1126/science.1200488

Fu, F. and Wang, Q., Removal of heavy metal ions from wastewaters: A review, *J. Environ. Manage.,* 92(3), 407–418 (2011). https://doi.org/10.1016/j.jenvman.2010.11.011

Ghaffour, N., Missimer, T. M. and Amy, G. L., Technical review and evaluation of the economics of water desalination: Current and future challenges for better water supply sustainability, *Desalin.,* 309, 197–207 (20131). https://doi.org/10.1016/j.desal.2012.10.015

Jones, E., Qadir, M., Vliet, v. M. T. H., Smakhtin, V. and Kang, S. M., The state of desalination and brine production: A global outlook, *Sci. Total Environ.,* 657, 1343–1356 (2019). https://doi.org/10.1016/j.scitotenv.2018.12.076

Kumar, R., Rauwel, P. and Rauwel, E., Nanoadsorbants for the removal of heavy metals from contaminated water: Current scenario and future directions, *Processes*, *9*(8), 1379 (2021). https://doi.org/10.3390/pr9081379

Mehta, D., Mazumdar, S. and Singh, S. K., Magnetic adsorbents for the treatment of water/wastewater—A review, *J. Water Process Eng.,* 49, 102938 (2022). https://doi.org/10.1016/j.jwpe.2015.07.001

Patel, H., Fixed-bed column adsorption study: A comprehensive review, *Appl. Water Sci.,* 9, 45 (2019). https://doi.org/10.1007/s13201-019-0927-7

Raji, Z., Karim, A., Karam, A. and Khalloufi, S., Adsorption of heavy metals: mechanisms, kinetics, and applications of various adsorbents in wastewater remediation—a review, *Waste*, 1(3), 775-805 (2023). https://doi.org/10.3390/waste1030046

Rao, A. V. R., Srividya, R., Bhemavarapu, R., Rejinthala, R., Karthik, P. and Daisy, E., Transforming Farm Agro Waste into Valuable resources: a guide to sustainable agriculture and economic growth, *From Waste to Wealth,* 989-1012 (2024). https://doi.org/10.1007/978-981-99-7552-5_44

Saida, -Al. B., Sandouqa, A., Shawabkeh, R. A. and Hussein, I., Synthesis of nanosilica for removal of Cd^{2+} and Cu^{2+} ions from aqueous solutions, *Mol.,* 27(21), 7536 (2022). https://doi.org/10.3390/molecules27217536

Shannon, M. A., Bohn, P. W., Elimelech, M., Georgiadis, J. G., Mariñas, B. J. and Mayes, A. M., Science and technology for water purification in the coming decades, *Nat.,* 452, 301–310 (2008). https://doi.org/10.1038/nature06599

Sharma, P., Kaur, H., Sharma, M. and Sahore, V., A review on applicability of naturally available adsorbents for removal of hazardous dyes and metals from wastewater, *Environ. Monit. Assess.,* 193, 185 (2021). https://doi.org/10.1007/s10661-011-1914-0

Singh, N. B., Nagpal, G., Agrawal, S. and Rachna., Water purification by using adsorbents: A review, *Environ. Technol. Innov.,* 11, 187–240 (2018). https://doi.org/10.1016/j.eti.2018.05.006

Singh, A., Chaudhary, S. and Dehiya, B. S., Fast removal of heavy metals from water and soil samples using magnetic Fe3O4 nanoparticles, *Environ. Sci. Pollut. Res.,* 28(4), 3942-3952 (2021). https://doi.org/10.1007/s11356-020-10737-9

Subramani, A. and Jacangelo, J. G., Emerging desalination technologies for water treatment: A critical review, *Water Res*., 75, 164-187 (2015). https://doi.org/10.1016/j.watres.2015.02.032

Sun, S., Zeng, H., Robinson, D. B., Raoux, S., Rice, P. M., Wang, S. X. and Li, G., Monodisperse MFe_2O_4 (M = Fe, Co, Mn) nanoparticles, *J. America. Chem. Soc.,* 126(1), 273–279 (2004). https://doi.org/10.1021/ja0380852

Tiwari, S., Hasan, A. and Pandey, L. M., A novel bio-sorbent comprising encapsulated Agrobacterium

fabrum (SLAJ731) and iron oxide nanoparticles for removal of crude oil co-contaminant, lead Pb (II), *J. environ. Chem. Eng.*, *5*(1), 442-452 (2017). https://doi.org/10.1016/j.jece.2016.12.017

Zhang, J., Zhai, J., Zheng, H., Li, X., Wang, Y., Li, X. and Xing, B., Adsorption, desorption and coadsorption behaviors of sulfamerazine, Pb (II) and benzoic acid on carbon nanotubes and nano-silica, *Sci. Total Environ.*, *738*, 139685 (2020). https://doi.org/10.1016/j.scitotenv.2022.152929